Unsteady aerodynamic effects in pitching airfoils studied through large-eddy simulations

Prabal S. Negi
Linné Flow Centre, KTH Mechanics
SE-100 44 Stockholm, Sweden
negi@mech.kth.se

Ricardo Vinuesa
Linné Flow Centre, KTH Mechanics
SE-100 44 Stockholm, Sweden
rvinuesa@mech.kth.se

Philipp Schlatter
Linné Flow Centre, KTH Mechanics
SE-100 44 Stockholm, Sweden
pschlatt@mech.kth.se

Ardeshir Hanifi
Linné Flow Centre, KTH Mechanics
SE-100 44 Stockholm, Sweden
ardeshir@mech.kth.se

Dan S. Henningson
Linné Flow Centre, KTH Mechanics
SE-100 44 Stockholm, Sweden
henning@mech.kth.se

ABSTRACT

Wall-resolved large-eddy simulations (LES) are utilized to investigate the flow physics of a wing section undergoing small amplitude pitch oscillations. A relaxation-term (RT) based filtering procedure is employed to add limited high order dissipation to account for the dissipation from the smallest scales which are not resolved. Validation of the procedure is presented for channel flows at $Re_\tau = 395$ for flow around a wing section at $Re_c = 400,000$. The procedure is then used for the simulation of small-amplitude pitching wing at $Re_c = 100,000$ with a reduced frequency $k = 0.5$. The investigation of the unsteady phenomenon is done in the context of a Natural Laminar Flow (NLF) wing, the performance of which depends critically on the suction side transition characteristics. The dynamic range of the pitch cycle sees the appearance, destabilization and disappearance of a laminar separation bubble at the leading edge. Abrupt changes are seen in the lift coefficient through the cycle, which are linked to a rapid movement of the transition point over the suction side. Destabilization of the laminar separation bubble is the cause of these rapid transition movements which are concentrated in a small region in phase space when the motion of the airfoil is close to the point of maximum angle of attack. Two widely different convective velocities are observed for the motion of structures across the airfoil surface.

INTRODUCTION

An abundance of articles can be found in the literature regarding flow over pitching wings. A large focus of the studies tends towards large pitch amplitudes and stall dynamics, with early experimental work by McCroskey *et al.* (1982), Carr *et al.* (1977) providing much of the initial understanding about the phenomenon. More recent works by Dunne & McKeon (2015), Rival & Tropea (2010), Choudhry *et al.* (2014) etc. continue the investigation of the process. Reviews by McCroskey (1982) and a more recent one by Corke & Thomas (2015) provide an overview of the development of unsteady airfoil behavior. Relatively little attention has gone towards studying unsteady aerodynamic behavior in the case of small pitch amplitudes. Some works dealing with small pitch amplitudes include the work done by Pascazio *et al.* (1996) which shows a time delay in laminar-turbulent transition in cases of moderate pitching frequencies and small pitch amplitudes (before the stall region). Nati *et al.* (2015) study the effect of small amplitude pitching on a laminar separation bubble at low Reynolds numbers.

Such cases qualitatively represent small changes in operating conditions, such as structural deformations of the wing or small trailing edge flap deflections. The understanding of flow response to such changes can be crucial in cases where such small perturbations can induce large changes in aerodynamic forces. The aerodynamic performance of Natural Laminar Flow (NLF) airfoils critically depends on maintaining laminar flow over the suction side of the airfoil and such airfoils can exhibit sensitive dependence on the transition location, viz. the operating conditions. In our current work we study the effect of small pitch oscillations on one such laminar airfoil, which was designed at the aerodynamics department of KTH (figure 1). The simulations were performed at "off-design" conditions where the laminar airfoil displays the above mentioned sensitivity to operating conditions as can be seen from the moment curve for steady angles of attacks in figure 2, which shows a sharp rise in C_m at an angle of attack $\alpha = 6^\circ$.

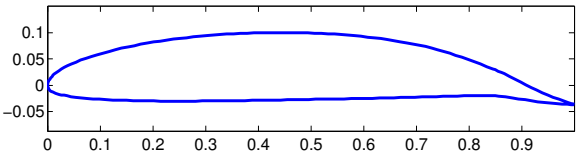

Figure 1: Natural Laminar Flow (NLF) airfoil used in the current study.

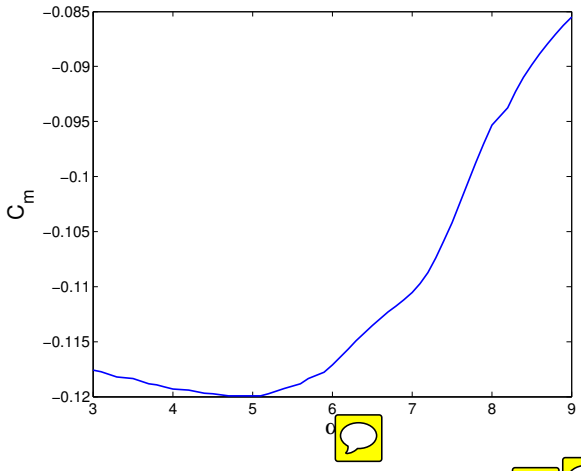

Figure 2: Coefficient of moment (C_m) obtained from xfoil for an NLF airfoil.

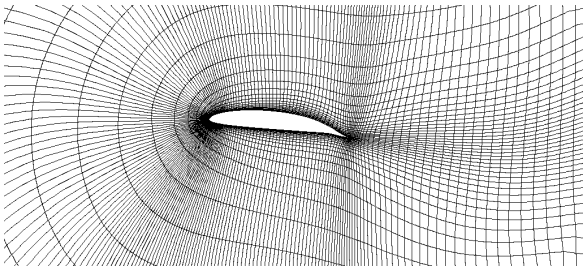

Figure 3: 2D section close up of the Spectral element grid around the airfoil.

Recent works with wall-resolved large-eddy simulations have proven to be an effective tool for studying flow physics at high Reynolds numbers but with a computational cost which is much lower than that of Direct Numerical Simulations (DNS). Some of the works to utilize this method include spatially evolving boundary layers Amor *et al.* (2014), channel flows Chin *et al.* (2015) and flow over wings Uzun & Hussaini (2010), Lombard *et al.* (2016). Successful application of the approach has motivated the present work which aims to gain insight into the flow physics of unsteady airfoils undergoing small amplitude pitch oscillations at a chord based Reynolds number of $Re_c = 100,000$.

A relaxation term based filtering approach is used ~~as an LES procedure~~ which reduces the computational cost of the simulation by an order of magnitude in comparison to a Direct Numerical Simulation (DNS) at the same Reynolds number. Quantitative comparisons of the procedure is validated for a channel flow at $Re_\tau = 395$ and for flow around a (stationary) wing section at $Re_c = 400,000$.

NUMERICAL METHOD

The computational code used for the simulations is Nek5000, which is an open source research code developed by Fischer *et al.* (2008) at Argonne National Labs. It is a based on a spectral-element method which allows the mapping of elements to complex geometries along with a high order spatial discretization within the elements. The method uses tensor-product arrangements of orthogonal tensor-product polynomials as basis functions and utilizes a Gauss-Lobatto-Legendre (GLL) quadrature for the distribution of points within the elements. The spatial discretization is done by means of the Galerkin approximation, following the $P_N - P_{N-2}$ formulation. An 11^{th} order polynomial interpolation is used within the spectral elements. The nonlinear terms are treated explicitly by third-order extrapolation (EXT3), whereas the viscous terms are treated implicitly by a third-order backward differentiation scheme (BDF3). Aliasing errors are removed with the use of over-integration. Nek5000 is written in Fortran 77 and C with efficient scaling for up to 1 million MPI ranks. The code has been acknowledged in more than 200 journal articles. The simulations were carried out on the Cray XC40 system Beskow at the PDC Center from KTH in Stockholm (Sweden).

RELAXATION TERM LES (RT-LES)

The LES method is based on the ADM-RT approach first used by Schlatter *et al.* (2006). The method supplements the governing equations with a dissipative term ($\chi\mathscr{H}(u)$). The equations of motion for the resolved velocity and pressure thus read:

$$\frac{\partial u}{\partial t} + u\cdot\nabla u = -\frac{1}{\rho}\nabla p + \frac{1}{Re}\nabla^2 u - \chi\mathscr{H}(u) \quad (1)$$

$$\nabla\cdot u = 0 \quad (2)$$

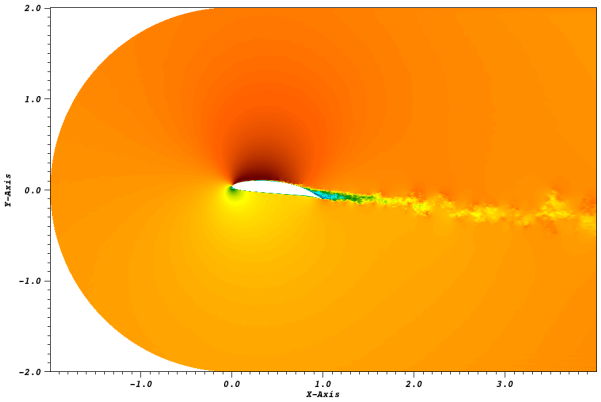

Figure 4: Simulation domain: Outflow boundary is 4 chords downstream of the airfoil while the inflow boundary is 2 chords away.

where $\mathscr{H}$ is a defined high pass spectral filter and χ is a model parameter which together with δ determines the strength of the dissipative term. The method has been used in earlier studies of boundary layer simulations in Argen *et al.* (2014) and Schlatter *et al.* (2006), and has been shown to be reliable in predicting transition location and also preserving the characteristic structures which are seen in the DNS of transitional flows (Schlatter *et al.* (2006)).

COMPUTATIONAL SETUP

A number of tests were carried out in a channel flow at $Re_\tau = 395$ and the results are compared with the DNS data of Moser *et al.* (1999) at the same Reynolds number. Finally the chosen resolution was set to $\Delta x^+ = 18$, $\Delta z^+ = 9$, with the first point in the wall normal direction set at $\Delta y_w^+ = 0.64$ and the wall normal resolution near the boundary layer edge is set at $\Delta y_{max}^+ = 11$. The resolution is very similar to the one used in Argen *et al.* (2014) where the ADM-RT model is also used to simulate a spatially evolving boundary layer up to $Re_\theta = 8300$. A comparison of the results for channel flow is shown in figure 5 for the mean velocity in figure 5 and for the kinetic energy budget in figure 6. Where, the superscript $^+$ indicates normalization in inner units. The dissipation shown in the figure is the total dissipation which is the sum of resolved dissipation and the added dissipation by the the relaxation term. The total dissipation matches the dissipation of the DNS data very well.

The same resolution (in inner units) is then used to design the mesh around the airfoil, with additional care taken for special regions like the leading and trailing edge. Wall shear stress data is obtained using Xfoil to estimate the grid spacing on the airfoil. A trip is introduced in Xfoil at $x/c = 0.05$ to obtain turbulent shear values on both the suction and pressure sides of the airfoil. Finally, the grid design uses the following criteria:

- For $0.1 < x/c < 0.6$, $\Delta x^+ = 18$, $\Delta y_{wall}^+ = 0.64$ and $\Delta y_{max}^+ = 11$, using the local wall shear (u_τ) values on the airfoil. Since the flow is expected to be laminar on the pressure side, the streamwise resolution is slightly relaxed to $\Delta x^+ = 25$ while keeping the same wall normal resolution.
- For $x/c < 0.1$, the peak u_τ value over the suction side of the airfoil is used to estimate the grid spacing.
- for $x/c > 0.6$, the suction side experiences a large adverse pressure gradient which reduces u_τ values. Therefore, the u_τ values from the pressure side are used for both the suction and

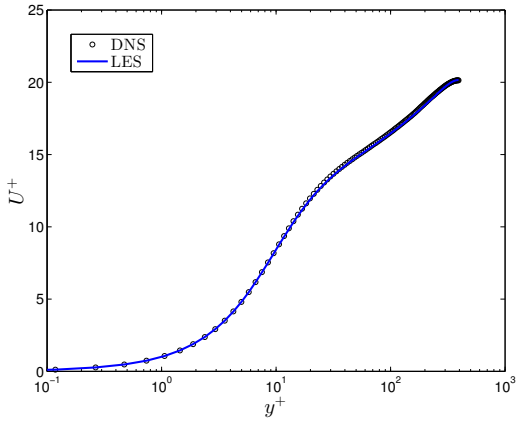

Figure 5: Comparison of mean velocity profile normalized in inner units.

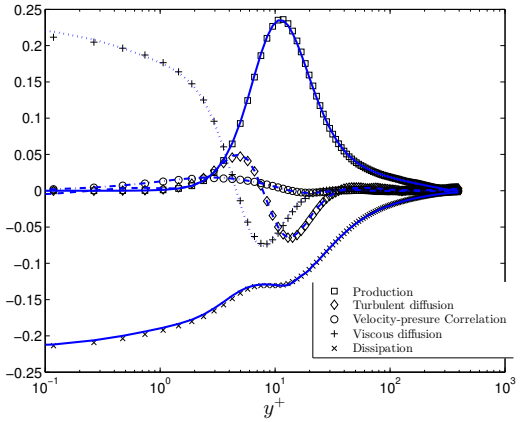

Figure 6: Comparison of kinetic energy budget normalized in inner units. Symbols represent the DNS data while the lines represent the values from the LES simulation.

pressure sides.

- Since the mesh is a structured C-grid type mesh, which is extruded in the span-wise direction, the span-wise resolution is constant throughout the domain. The resolution is set to $\Delta z^+ = 9$, where the u_τ value is taken to be the peak value on the suction side.

A different criterion is needed for defining the resolution in the wake where the wall based criteria do not hold. Accordingly, RANS simulations are performed in fluent to estimate the kolmogorov length scale (η) in the wake region. The grid in the wake region is designed such that the average grid spacing between the GLL points follows the criteria: $\Delta x/\eta < 9$. A close up of grid near the airfoil can be seen in figure 3. The far field boundaries are 2 chords away from the airfoil in either direction and the downstream boundary is 4 chords downstream from the airfoil. The inlet is designed as a curved inflow boundary with a constant radial distance of 2 chords from the leading edge of the airfoil. The domain extends to 0.25 chords in the spanwise domain. The domain can be visualized in figure 4 which shows the spectral element distribution in the domain. Each of the spectral elements are further discretized by $12 \times 12 \times 12$ grid points in 3D, corresponding to an 11^{th} order spectral discretization. Periodic boundary conditions are imposed on the span-wise boundaries, while the dong outflow condition is imposed on the outflow boundaries. The dong outflow boundary is shown

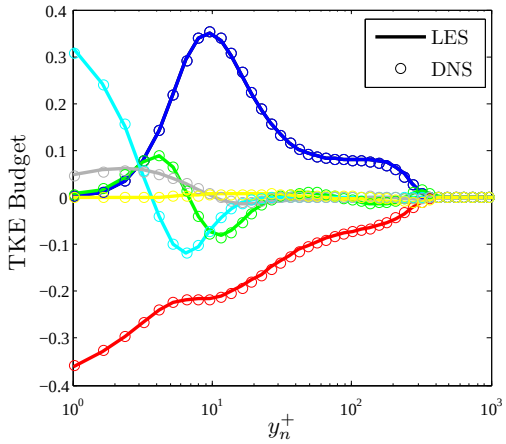

Figure 7: Comparison of kinetic energy budget for a NACA4412 wing section at the suction side location of x/C=0.7. The circles represent DNS data from Hosseini *et al.* (2016) while the lines are data from the LES simulation. The individual terms are color coded as: Production, Dissipation, Viscous diffusion, Turbulent diffusion, Velocity-Pressure correlation, Convection

to be accurate and stable in flows with strong back-flow velocities at the outflow boundary ~~Dong *et al.* (2014)~~. Data is extracted from an unsteady RANS simulation and the time averaged value is interpolated onto the domain inlet and far-field boundaries. The interpolated data is then imposed as a Dirichlet boundary conditionon these boundaries. The method is very similar to the one used by Hosseini *et al.* (2016) in their DNS of flow around a wing section. In order to simulate low turbulence flight conditions, free-stream turbulence of turbulence intensity $Ti = 0.1\%$ is superimposed on the Dirichlet boundary conditions. The free-stream turbulence is generated using fourier modes with a von-karman spectrum. The procedure is similar to the one used in Brandt *et al.* (2004) and has been used for the study of transition in flat plate boundary layers under the influence of free-stream turbulence.

A validation of the above criterion for complex geometries such as a wing section is performed at a chord based Reynolds number of $Re_c = 400,000$ for NACA4412 airfoil. The LES grid resolution is setup with the same grid criteria as described above. The domain boundaries and boundary conditions are identical to the setup in Hosseini *et al.* (2016). The results are validated using the DNS data from Hosseini *et al.* (2016) for the same airfoil and Reynolds number. The normalized kinetic energy budget is shown in figure 7. LES profiles (lines) match very well with the DNS data (circles). The profiles are from the suction side of airfoil with the stream-wise location being $x/C = 0.7$.

STEADY SIMULATIONS

Steady simulations are performed to investigate the location of transition without pitching motion. The results are consistent with the trends observed from xfoil showing a large movement of the transition point within a small α change. Steady simulations are performed for $Re_c = 100,000$ at two different angles of attack ($\alpha = 6.7^\circ$ and $\alpha = 8.0^\circ$). As observed in figure 8, the iso-contours of λ_2 structures show a substantial change in transition location for a small $\Delta\alpha = 1.3^\circ$. For $\alpha = 6.7^\circ$ the transition is close to the trailing edge at $x/C \approx 0.7$, where the effects of strong pressure gradient and trailing edge separation are dominant. While for $\alpha = 8.0^\circ$ the

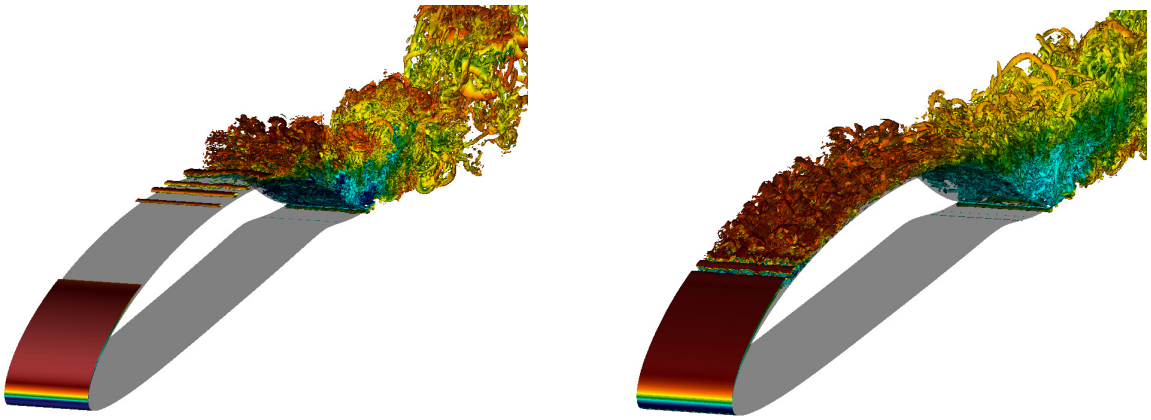

(a) $\alpha = 6.7^\circ$ (b) $\alpha = 8.0^\circ$

Figure 8: λ_2 structures for different (steady) angles of attack for a NLF airfoil.

transition has moved close to the leading edge at $x/C \approx 0.2$. Formation of a laminar separation bubble can be observed at $\alpha = 8.0^\circ$, which is the cause of transition. The separation bubble is absent in the lower $\alpha = 6.7^\circ$ case.

PITCHING RESULTS

Once the transition change is established in the steady simulations, the airfoil is then pitched about a mean $\alpha = 6.7^\circ$ with a pitching amplitude of $\Delta\alpha = 1.3^\circ$ and a reduced frequency of $k = \frac{\omega C}{2U_\infty} = 0.5$. Where ω is the angular frequency of oscillation, C is the chord length, and U_∞ is the free-stream velocity. The motion of the airfoil is prescribed by equation 3:

$$\alpha = 6.7^\circ + 1.3^\circ \sin(\omega t) \tag{3}$$

The variation of the coefficient of lift with time is shown in figure 9 where the blue line shows the C_L values and the dashed black line shows the variation of α with time. The initial phase of pitching motion is carried out using a lower polynomial order ($N = 5$) to simulate the transient period of the flow at a lower computational cost. The polynomial order is then smoothly raised to $N = 11$ before the fourth pitch cycle. The qualitative behavior of the lift coefficient between the third and the fourth pitch cycle do not change, where the lift coefficient shows a smooth ramp up during the pitch up motion, with secondary effects occurring close to the maximum angle of attack. Due to the fairly large separation at the trailing edge and effects of transition movement, we do not expect successive pitch cycles to have identical behavior, however qualitative trends appear to be similar and are captured by both the low and high polynomial order pitch cycles.

A space-time plot of the instantaneous span-wise averaged skin-friction coefficient (C_f) is shown in figure 12a which spans the fourth pitch cycle in time. The plot indicates the region of turbulent flow over the airfoil as a function of time. Regions with color intensity strongly towards red show regions of high shear and thus turbulent flow. The exception to the rule being the region close to the leading edge where the flow is laminar but a high shear region exists due to the strong curvature and flow acceleration effects. Inclined streaks of alternating red and blue patterns are signatures of the motion of strong vorticies over the airfoil surface, which leave an alternating imprint of positive and negative shear-stress on the wall. Evident from the red colored regions is the abrupt upstream

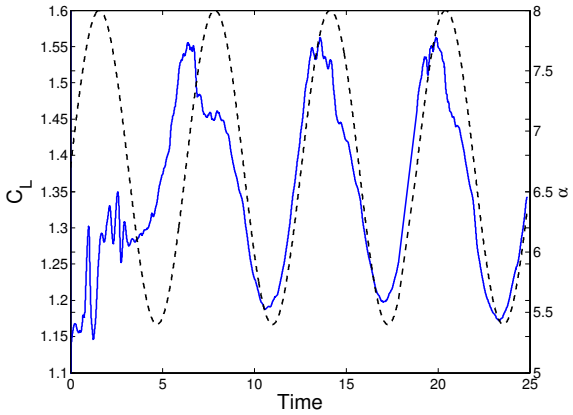

Figure 9: Coefficient of Lift (C_L-) and angle of attack ($\alpha--$) variation with time. C_L is on the left axes while α is on the right axes.

motion of the start of the high shear region at $T \approx 21$. This signifies the sharp movement of the transition point. The cause for the sharp transition movement can be found in the instability of the laminar separation bubble. A phase plot of C_L *vs* α (figure 10) for the last two pitch cycles also shows a sudden drop in the integral value which occurs when the pitch cycle is close to the maximum angle of attack.

Dynamics of the separation bubble can be seen in figure 12b, which shows the space time evolution of negative shear stress. Black colored regions indicate negative shear stress and thus indicative of separated flow. The LSB first appears at $T = 19.73$ during the upward pitch cycle, gradually growing in size and eventually becomes unstable. On the downward cycle ($T = 20.4 - 23.56$) the bubble undergoes the opposite behavior, whereby it ceases to be unstable and slowly shrinks in size to eventually disappear at $T = 22.96$. The turbulent region is also seen to visibly detach from the separation bubble and is slowly convected downstream. This rear-front of the turbulent region convects downstream as seen in figure 12a with its convection velocity marked by a red arrow. The downstream convection occurs at a nearly constant velocity of $U_{conv} \approx 0.17$. This is ~~in contrast with~~ the convection velocity of the strong coherent vorticies (alternating red and blue streaks in figure 12a) which also move at a near constant, but much higher convection velocity of $U_{conv} \approx 0.59$ (blue arrow).

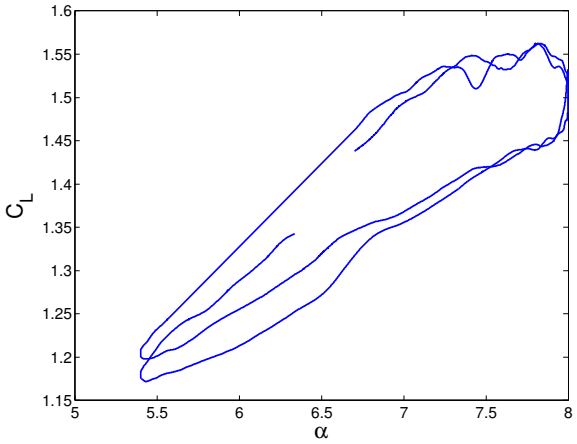

Figure 10: Phase portrait of C_L and α. The sense of the motion is clockwise.

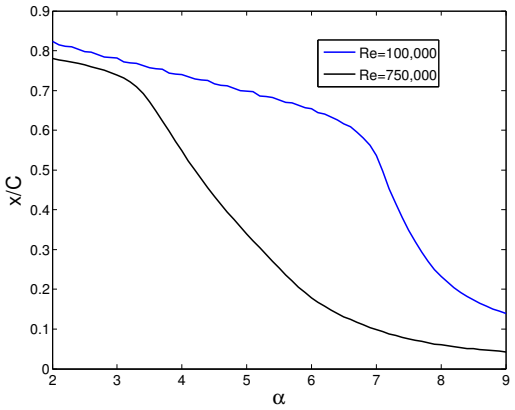

Figure 11: Reynolds number variation of suction side transition location.

HIGHER REYNOLDS NUMBER Some insight can be gained on Reynolds number trends from the integral boundary code xfoil, which indicates the movement of transition location from a point close to the trailing edge to a point close to the leading edge also occurs at higher Reynolds numbers of $Re_c = 750,000$ (figure 11). However at higher Reynolds numbers the separation bubble is expected to be too small to play a significant role. The transition location is then expected to be determined by the instability of Tollmien-Schlichting (TS) waves, which will be the dominant source of instability. However as indicated by the xfoil data, even TS instability location changes rapidly with a small $\Delta\alpha$ near $\alpha \approx 3.5°$. The effect of pitch oscillations on TS wave instability may again alter the aerodynamic performance of the airfoil.

SUMMARY AND CONCLUSION

A relaxation term filtering procedure is used for wall-resolved LES of flow over a pitching airfoil. The procedure complements Navier Stokes equations with a dissipative term which is built using a high-pass filtered velocity field. The role of the term is to compensate for the missing dissipation from the highest unresolved scales of turbulence. Validation of the LES procedure is done in a channel flow at $Re_\tau = 395$ and for a wing section at a chord based Reynolds number of $Re_c = 400,000$. The results show a very good match when compared with the available DNS data sets of Moser *et al.* (1999) and Hosseini *et al.* (2016).

Flow over an airfoil is then simulated using the LES procedure at a chord based Reynolds number of $Re_c = 100,000$. The airfoil chosen is an NLF airfoil, designed the aerodynamics department of KTH, which displays sharply changing characteristics in the off-design operating conditions. Specifically, the transition location moves from $x/C \approx 0.7$ to $x/C \approx 0.2$ within a 1.3° change in angle of attack. Such a change in transition location is reproduced in the steady simulations.

Pitching the airfoil within this dynamic range displays a rich variety of unsteady physical phenomena. In the pitching cycle when the airfoil is near the mean angle of attack, no laminar separation bubble is present near the leading. However vortex shedding can be observed near $x/C \approx 0.6$, which is also approximately the start of high adverse pressure gradient region on suction side of the airfoil surface. These vorticies leave alternating positve and negative imprint on the wall-shear, and convect downstream at a near constant velocity of $U_{conv} \approx 0.59$. The point of vortex shedding slowly moves upstream as the airfoil goes through its pitch up cycle. The laminar separation bubble appears at the leading edge and grows in size, eventually becoming unstable and causing the transition near $x/C \approx 0.2$. Destabilization of the separation bubble occurs when the pitch cycle is close to it's maximum angle of attack and the upstream motion of transition is abrupt. This also causes a sudden change in the coefficient of lift experienced by the airfoil. During the pitch down motion, the opposite effects occur in the separation bubble where it ceases to be unstable, shrinks in size and eventually disappears. When the separation bubble stops being a source of turbulence, the transition point detaches from the bubble and slowly convects downstream and the flow over the suction side undergoes a slow relaminarization. The last wave-packet of turbulent flow which detached from the separation bubble convects downstream at a nearly constant convection speed of $U_{conv} \approx 0.17$, ~~which is in sharp contrast with the convection velocity seen earlier for the shed vorticies when the flow was laminar.~~

Characteristics of the NLF airfoil change with Reynolds number, however the rapid change in transition location is still predicted at higher Reynolds numbers. At these Reynolds numbers however, transition mechanism will be fundamentally different since TS wave transition would be the dominating mechanism. The response of boundary layer TS wave transition to small-amplitude pitching again remains unknown in such cases where the transition location is highly sensitive. The numerical setup is under way to simulate small-amplitude pitch oscillation at higher Reynolds numbers.

ACKNOWLEDGEMENT

The computations were performed on resources provided by the Swedish National Infrastructure for Computing (SNIC) at the PDC Center for High Performance Computing at the Royal Institute of Technology (KTH). We would like to thank Dr. David Eller and Mikaela Lokatt for providing us with the NLF design and the numerous discussion on different aerodynamic aspects of the project.

REFERENCES

Amor, Georg Eitel, Örlü, Ramis & Schlatter, Philipp 2014 Simulation and validation of a spatially evolving turbulent boundary layer up to $re_\theta = 8300$. *International Journal of Heat and Fluid Flow* **47**, 57–69.

Brandt, Luca, Schlatter, Phlipp & Henningson, Dan S. 2004 Transition in boundary layers subject to free-stream turbulence. *Journal of Fluid Mechanics* **517**.

Carr, Lawrence W, McAlister, Kenneth W & McCroskey, William J 1977 Analysis of the development of dynamic stall based on oscillating airfoil experiments. *Tech. Rep.*.

Chin, C., Ng, H.C.H., Blackburn, H.M., Monty, J.P. & Ooi, A.

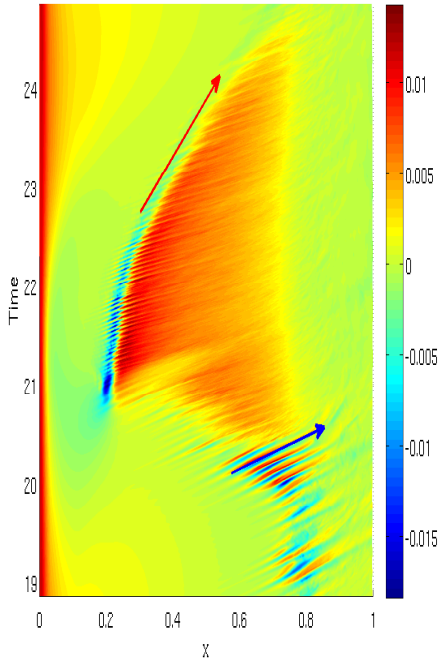

(a) Space-time variation of skin-friction coefficient (C_f)

.

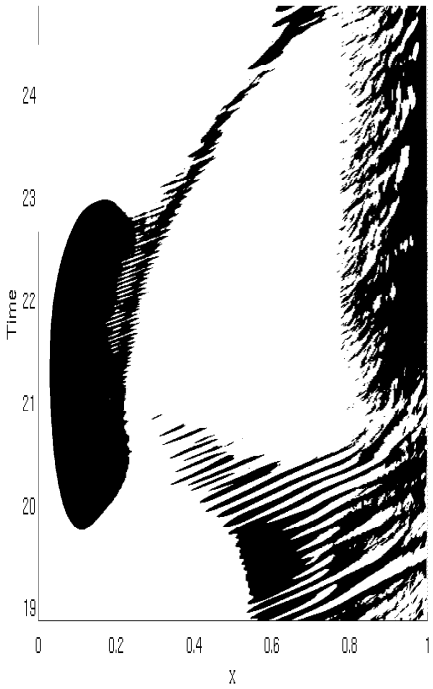

(b) Black regions indicate negative skin fiction values

Figure 12: Space-time plot for skin-friction coefficient (C_f) and separated flow regions. The values are obtained from the instantaneous flow averaged over the span-wise direction.

2015 Turbulent pipe flow at $Re_\tau = 1000$: A comparison of wall-resolved large-eddy simulation, direct numerical simulation and hot-wire experiment. *Computers and Fluids* **122**, 26 – 33.

Choudhry, Amanullah, Leknys, Ryan, Arjomandi, Maziar & Kelso, Richard 2014 An insight into the dynamic stall lift characteristics. *Experimental Thermal and Fluid Science* **58**, 188 – 208.

Corke, Thomas C. & Thomas, Flint O. 2015 Dynamic stall in pitching airfoils: Aerodynamic damping and compressibility effects. *Annual Review of Fluid Mechanics* **47** (1), 479–505.

Dong, Suchuan, Karniadakis, George E & Chryssostomidis, C 2014 A robust and accurate outflow boundary condition for incompressible flow simulations on severely-truncated unbounded domains. *Journal of Computational Physics* **261**, 83–105.

Dunne, Reeve & McKeon, Beverley J. 2015 Dynamic stall on a pitching and surging airfoil. *Experiments in Fluids* **56** (8), 157.

Fischer, P. F., Lottes, J. W. & Kerkemeier, S. G. 2008 nek5000 web page. Http://nek5000.mcs.anl.gov.

Hosseini, S. M., Vinuesa, R., Schlatter, P., Hanifi, A. & Henningson, D. S. 2016 Direct numerical simulation of the flow around a wing section at moderate Reynolds number. *International Journal of Heat and Fluid Flow* **61, Part A**, 117 – 128.

Lombard, J.-E. W., Moxey, D., Sherwin, S. J., Hoessler, J. F. A., Dhandapani, S. & Taylor, M. J. 2016 Implicit Large-Eddy Simulation of a Wingtip Vortex. *AIAA Journal* **54**, 506–518.

McCroskey, WJ, McAlister, KW, Carr, LW & Pucci, SL 1982 An experimental study of dynamic stall on advanced airfoil sections. volume 1: Summary of the experiment. *Tech. Rep.*.

McCroskey, W J 1982 Unsteady airfoils. *Annual Review of Fluid Mechanics* **14** (1), 285–311.

Moser, Robert D., Kim, John & Mansour, Nagi N. 1999 Direct numerical simulation of turbulent channel flow up to $Re_\tau = 590$. *Physics of Fluids* **11** (4), 943–945.

Nati, A, De Kat, R, Scarano, F & Van Oudheusden, BW 2015 Dynamic pitching effect on a laminar separation bubble. *Experiments in Fluids* **56** (9), 172.

Pascazio, M, Autric, J, Favier, D & Maresca, C 1996 Unsteady boundary-layer measurement on oscillating airfoils-transition and separation phenomena in pitching motion. In *34th Aerospace Sciences Meeting and Exhibit*, p. 35.

Rival, David & Tropea, Cam 2010 Characteristics of pitching and plunging airfoils under dynamic-stall conditions. *Journal of Aircraft* **47** (1), 80–86.

Schlatter, Philipp, Stolz, Steffen & Kleiser, Leonhard 2006 Large-eddy simulation of spatial transition in plane channel flow. *Journal of Turbulence* **7**, N33.

Uzun, A. & Hussaini, M. Y. 2010 Simulations of vortex formation around a blunt wing tip. *AIAA Journal* **48**, 1221–1234.